A Whole-cell Model to Simulate
Mercuric Ion Reduction by *E. coli* under Stationary and Perturbed Conditions

G. Maria[*]

Laboratory of Chemical & Biochemical Reaction Engineering
University Politehnica of Bucharest, P.O. 35-107 Bucharest, Romania

Gram-negative bacteria display mercury resistance conferred by the plasmid encoded *mer* operon. A genetic regulatory circuit (GRC), inducible by the presence of mercury compounds in the environment, allows controlling the expression of at least 6-7 *mer* genes producing enzymes responsible for the mercuric ions transport and reduction. In spite of extensive studies on bacterial toxic metal resistance, few and rather unstructured kinetic models have been proposed to characterize the process dynamics. This paper aims at proposing an extended dynamic model, of modular construction, to reproduce the characteristics of GRC controlling the mercury uptake and reduction process. The illustrated case study uses experimental data from literature collected on cultures of *E. coli* cells cloned with the plasmid R100 to increase the source of *mer* operon. The available information is used to fit the model parameters and to adjust the GRC properties. The pathway includes seven regulatory modules placed in an *E. coli* growing cell on which response to external perturbations is studied. The model, accounting for the variable cell volume under isotonic conditions, can reproduce the GRC dynamic control in connection with the cell content replication, and various cell behaviours such as *mer* gene expression amplification at low levels of external stimuli, or cell content 'ballast' effect when coping with stationary or dynamic perturbations.

Key words:
Bacterial mercury resistance, genetic regulatory circuit, dynamic modelling

Introduction

The resistance of bacteria to metallic ions or organometallic compounds from environment is an extensively investigated subject, and a large number of studies and well-documented reviews are available on: bacterial resistance to mercury compounds;[1–3] bacterial resistance to silver;[4] bacterial control of Zn, Cu and Co availability;[5–6] copper homeostasis control in bacteria under a changing environment;[7–8] bacterial iron homeostasis;[9–10] nickel uptake and utilization by microorganisms;[11] manganese metabolism in bacteria;[12] bacterial/prokaryotic metal resistance.[13–16] Specific genes are identified in various microorganisms as being responsible with the inorganic or organic metal compound transport and metabolisation (uptake and utilization). Such extensive studies will eventually lead to a catalog of bacteria specifically adapted to toxic metals and of metal-responsive genes. Study of the effect of metal-contaminants on various organisms is of high interest due to a large spectrum of practical implications in medicine, food chemistry, environmental engineering, and agriculture. Large-scale applications are reported, such as efficient mercury removal from wastewaters by microorganisms.[17–19]

The resistance to mercury compounds is one of the most widely observed phenotypes in eubacteria for many decades. This is one of the most interesting bacterial defence systems against toxic mercuric pollutants, being extensively studied from various points of view, starting from metabolic/biochemical and genetic aspects to engineering applications in environmental bioremediation and biomonitoring (review of Barkay *et al.*[1]). Instead of building carbon- and energy-intensive disposal devices to get ride of toxic metallic-compounds, both Gram-positive and Gram-negative bacteria have developed a simpler and more efficient detoxification process by reducing the redox-active thiophilic metallic ions to monoatomic gas, less toxic and easily eliminable in the environment. Such a mechanism is based on the existing abundant cellular reservoir of thiolic and reductant compounds able to coordinate and then reduce Hg(II) to volatile metal, with the expense of cellular energy.

Responsible for such a process in bacteria is the *mer* operon, the expression of which is induced by the presence of cytosolic Hg(II). The *merRTPCA(B)D* gene expression leads to production of PmerP, PmerT, and PmerC (or PmerB) enzymes necessary to transport the mercuric compounds into the cytosol, and of PmerA enzyme

---

[*] Email: gmaria99m@hotmail.com

catalysing its reduction. The tight cross- and self-control of *mer* operon expression by means of PmerR and PmerD enzymes ensures a quick response to the presence of mercury in the environment and an efficient detoxification process (in the present study G• denotes genes, while P• denotes proteic enzymes).

The current state-of-the-art in kinetic modelling of *E. coli* resistance to mercury includes Michaelis-Menten unstructured kinetics for the membranar transport and enzymatic reduction steps. As the involved reductant NADPH and thiol redox buffers RSH are present in excess, the only intracellular species accounted in the rate expression is the cytosolic Hg(II) of concentration resulting from the transport and reduction step mass balances.

Modelling such a complex process at a cellular level on a structured basis, with a degree of detail accounting for species involved in the metabolic pathway and in the GRC ensuring the *mer* operon expression regulation, is not an easy task. This is because such a model needs to include all relevant reaction steps and intermediates in the reaction pathway, but also to reproduce all connections of the GRC with the rest of the cell responsible for the holistic response of the bacteria to various perturbations from environment under a continuous cell-volume growth and content replication.

The whole-cell approach to dynamically represent the GRC characteristics has been treated in the literature by using continuous, Boolean, or stochastic variables, in a structured modelling accounting for individual or lumped transcription factors (TF), intermediates, metabolites, etc.[20–22] Most of them use classical modelling framework of a constant volume and constant osmotic pressure system, accounting for the cell-growing rate as a 'decay' rate of key-species (often lumped with the degrading rate) in a so-called 'diluting' rate. Such a representation might be satisfactory for many applications, but not for accurate modelling of cell regulatory /metabolic processes under perturbed conditions, or for division of cells, distorting the prediction quality. The variable-volume whole-cell (VVWC) modelling framework, by explicitly linking the volume growth, external conditions, osmotic pressure, cell content ballast and net reaction rates for all cell-components, is proved more promising in predicting local and holistic properties of the metabolic network.[22–26]

The modelling effort can be backed by the recently advanced concepts of *reverse engineering* and *integrative understanding,* which are useful tools for deciphering the whole cell metabolic and gene regulatory network. These techniques try to disassemble the system as much as possible, by performing tests, and learning about the structure of the whole and its parts and then trying to 'recreate' the same system from scratch. In the GRC case, such tests consist of deleting or altering the expression of a given gene, observing the outcome and using the models to reproduce the gene regulatory module and the network characteristics. The advantage is the possibility to reduce the system complexity and the size of the identification problem, for instance by understanding the gene expression response to a perturbation as the response of a few genetic regulatory loops instead of the response of thousands of genetic circuits in the metabolic pathway.

Because many cell regulatory systems are organized as modules (up to 23–25),[27] in developing the mentioned analysis the modular approach is preferred due to various advantages:[23–24] a separate analysis of modules in conditions that mimic the stationary and perturbed cell growth; investigation of module links used to construct the whole GRC of optimised regulatory efficiency that ensure key-species homeostasis and network holistic properties; investigation of GRC characteristics such as tight control of gene expression, a quick dynamic response and high sensitivity to specific inducers, and gene circuit robustness (i.e. a low sensitivity vs. undesired inducers).

The scope of this paper is to detail the mercuric ion reduction kinetic model in *E. coli* by including a modular and structured representation of the GRC controlling the inner cell process. The reproduced case study is that of Philippidis *et al.*[28] using *E. coli* cell cloned with the plasmid R100 to increase the source of *mer* operon. The reported experimental data are used to fit the model parameters and adjust the regulatory system properties. The paper also investigates the advantages of using VVWC deterministic approach, by placing the seven proposed regulatory modules (reproducing the mercury transport, reduction and operon expression control) in an *E. coli* growing cell. Thus, the GRC control in connection with the cell content replication can be mimicked under simulated stationary or perturbed environmental conditions. Certain cell behaviours, such as *mer* gene expression amplification at low levels of external stimuli, or cell content 'ballast' and 'inertial' effect when coping with perturbations are also possible to be simulated, the model predictions being adjusted by means of suitable parameters and levels of intermediate species.

The resulted GRC model can be useful not only for predicting the cell efficiency in coping with Hg(II)-ions under various environmental conditions, but also to elaborate complex cell simula-

tion platforms. The result is the possibility to *in-silico* design modified bacterial cells (cloned with plasmids), of desirable properties, leading to the improvement of the industrial bioprocess. This approach is in line with the new concept '*from gene to product*'[55] used in bioengineering, and focuses on improving the metabolic performances of the microorganisms used in the process industry, by understanding the cell metabolism and the GRC responsible with regulation of cell biochemical reactions, and then conferring new properties to a mutant cell (the co-called 'gene circuit engineering').[56,22]

The whole-cell model

Mercuric ion reduction mechanism in *E. coli*: Include species into a model

The basic mechanism for mercuric ion reduction in *E. coli* cell (a Gram-negative bacteria) is extensively reviewed in the literature.[1,28–32] The process is mediated by polypeptides/proteins (denoted

by P•), most of them resulted from Hg(II)-inducible *mer* operon expression. Based on literature information a reduced reaction pathway has been constructed and presented in Fig. 1, involving the main compounds and relevant lumps. The model accounts for seven regulatory modules that maintain the system homeostasis and control: i) Hg^{2+} transport from environment into cytosol across the membrane (catalysed by ET); ii) Hg^{2+} reduction to Hg^0 by PmerA; iii) proteome P and genome G replication (necessary to mimic the cell ballast inertial effect in the VVWC model);[22,24] iv) PmerR synthesis (PmerR is the transcriptional activator-repressor of other proteins and of itself synthesis); v) ET lumped protein synthesis; vi) PmerA reductase synthesis; vii) PmerD protein synthesis. The modular representation of the cell process is proved as being advantageous, by combining the modelling effort with a sensitivity analysis that relate the GRC/cell holistic properties to the structure, function and efficiency of certain components or individual modules to cope with perturbations.[22–24] The linking strategy of semi-autonomous modules ensures the
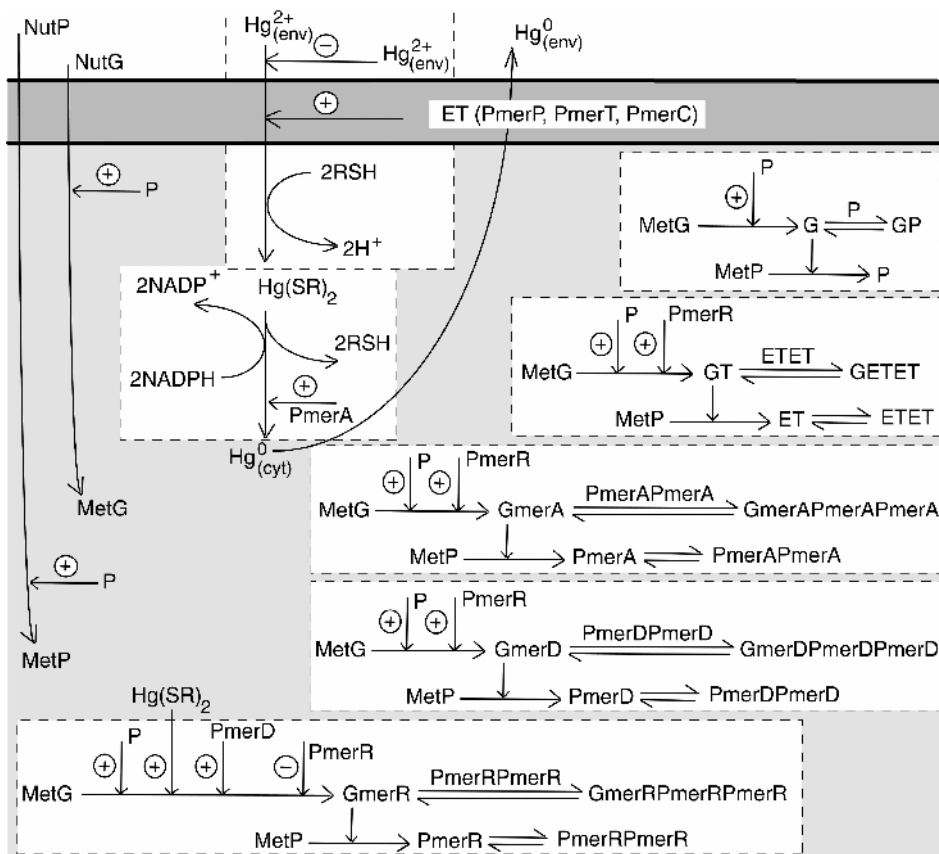

Fig. 1 – *Cell model: placing mer operon, i.e. a metal-responsive regulator (of expression controlled by PmerR protein), in a Gram-negative E. coli bacteria to reduce the reactive ionic Hg²⁺ to volatile, relatively inert Hg⁰ vapour. The model includes seven regulatory modules that maintain the system homeostasis (approx. marked-out by dashed rectangles). Notations: P = lumped proteome; G = lumped genome; NutG, NutP = lumped nutrients used for gene and protein synthesis; P• = proteins; G• = genes (see Table 1); RSH = low molecular mass cytosolic thiol redox buffer (such as glutathione); perpendicular arrows on the reaction path indicate the catalytic activation, repressing or inhibition actions; absence of a substrate or product indicates an assumed concentration invariance of these species; ⊕/⊖ positive or negative feedback regulatory loops.*

whole system homeostasis, optimum regulatory properties of the genetic regulatory chain, and optimized functions for each involved enzyme with efficient cell resource consumption. According to the intermediates' role and specific synthesis scheme,

temporal hierarchy and event succession into the cell can also be accounted for by such a modelling approach.

The proposed GRC model accounts for 26 individual or lumped species, being presented in Table 1

T a b l e 1 – *Stationary concentrations of individual and lumped species considered in the whole-cell model (E. coli cell with plasmid R100 as source of mer operon; Philippidis et al.[28,30–31] data for environmental $[Hg^{2+}]_{s,env}$ = 40 µM). Notations: 'env' = environment; 'cyt' = cytosol; 'o' = initial (born cell); 's' = stationary. Concentrations are expressed in nM referring to the cell volume or environmental space (*).*

Species	Role (Symbol in figures)	Stationary concentrations (nM)	Observations
$Hg^{2+}_{(env)}$	mercuric ion in the environment ($Hg^{2+}_{(env)}$)	40000 (*)	Philippidis et al.[28] case study
$Hg^{2+}_{(cyt)}$	mercuric ion in the cytoplasm ($Hg^{2+}_{(cyt)}$)	3430	Philippidis et al.[28] case study
$Hg^{0}_{(cyt)}$	free mercury in the cytoplasma ($Hg^{0}_{(cyt)}$)	3430	adopted as for $Hg^{2+}_{(cyt)}$
NutG	lumped nutrients used for genome synthesis (NutG)	$3 \cdot 10^7$ (*)	Maria,[22] Morgan et al.[25]
NutP	lumped nutrients used for proteome synthesis (NutG)	$3 \cdot 10^8$ (*)	Maria,[22] Morgan et al.[25]
MetG	lumped metabolites used for genome synthesis (MetG)	$2.0017 \cdot 10^7$	eq. (3)
MetP	lumped metabolites used for proteome synthesis (MetP)	$3 \cdot 10^8$	Maria,[22] Morgan et al.[25]
G	lumped genome (G)	4500/2	EcoCyc[37]
GP	catalytic inactive form of the lumped genome (GP)	4500/2	optimized
P	lumped proteome (P)	$1 \cdot 10^7$	EcoCyc[37]
GmerR	gene expressing the protein PmerR	3/2	Philippidis et al.[28] case study
PmerR	protein with catalytic role in the *mer* operon expression	1000	adopted
GmerRPmerRPmerR	catalytic inactive form of gene GmerR (GRPRPR)	3/2	optimized
PmerRPmerR	dimer of PmerR with TF role in the PmerR synthesis (PmRPmR)	0.1−6 (optimized)	role in controlling the gene activity[22,40]
GT	gene lump expressing the protein ET	3/2	Philippidis et al.[28] case study
ET	protein lump with catalytic role in the membranar transport of $Hg^{2+}_{(env)}$	6572	Barkay et al.[1] (see eq. 1)
GTETET	catalytic inactive form of gene GT	3/2	optimized
ETET	dimer of ET with TF role in the ET synthesis	0.1−6 (optimized)	role in controlling the gene activity[22,40]
GmerA	gene expressing the protein PmerA	3/2	Philippidis et al.[28] case study
PmerA	protein with catalytic role in the $Hg^{2+}_{(cyt)}$ reduction to $Hg^{0}_{(cyt)}$	3700	adopted the same with PmerP (see the text)
GmerAPmerAPmerA	catalytic inactive form of gene GmerR (GAPAPA)	3/2	optimized
PmerAPmerA	dimer of PmerA with TF role in the PmerA synthesis (PmAPmA)	0.1−6 (optimized)	role in controlling the gene activity[22,40]
GmerD	gene expressing the protein PmerD	3/2	Philippidis et al.[28] case study
PmerD	protein with activation role of PmerR synthesis (when inducer $Hg^{2+}_{(cyt)}$ starts to decline); also antagonist to PmerRPmerR repressing action	100	adopted following the observations of Barkay et al.[1]
GmerDPmerDPmerD	catalytic inactive form of gene GmerD (GDPDPD)	3/2	optimized
PmerDPmerD	dimer of PmerD with TF role in the PmerD synthesis (PmDPmD)	0.1−6 (optimized)	role in controlling the gene activity[22,40]

T a b l e 2 – *E. coli cell main characteristics*

Symbol	Value	Observations
$V_{cyt,0}$	$2.19 \cdot 10^{-16}$ L	initial cell volume (cytoplasma); adjusted to match the data of Philippidis *et al.*[28,30–31]
t_c	138.6 min	cell cycle time (adopted as for *Pseudomonas putida*, used for mercuric ion reduction).[19]
D_s	$D_s = \ln 2/t_c = 0.3 \text{ h}^{-1}$	average dilution rate
c_{cell}	$5 \cdot 10^{-10}$ cells (L env)$^{-1}$	cell concentration in the culture medium[28]
ρ_{cell}	10^6 mg protein (L cell)$^{-1}$	cell density in the culture medium

together with the stationary concentrations and functions. The cell main characteristics are presented in Table 2. Basically, the case study reproduces the experimental data of Philippidis *et al.*[28] for *E. coli* cell cloned with the plasmid R100 to increase the source of *mer* operon up to 3 copynumbers per cell (ca. 3 nM).[23]

The mercury reduction process is highly regulated by negative and positive regulatory loops disposed in a cascade control schema, working as an amplifier of the external stimuli (mercury), which activate but also modulate the *mer* operon expression according to external conditions. The result is a well-regulated metabolic pathway conferring cell resistance to mercuric ions (generically denoted by HgX_2, where X is a solvent nucleophile), or organo-mercuric compounds (such as CH_3HgX). For the mercuric ion resistance case, the *mer* operon (also denoted GmerRTPCAD) includes several genes encoding the following gene products:[1]

– GmerR encoding the protein PmerR, which activate and control the expression of all *mer* operon genes, and also negatively autoregulates its own transcription;

– GmerP, GmerT and GmerC, encoding transport proteins, i.e. the periplasmic PmerP, and the inner membrane PmerT and PmerC; GmerB gene encoding organomercurial lyase PmerB is activated only when environmental mercury is present as organic C-Hg type compounds;

– GmerA encoding the soluble mercuric reductase PmerA (Hg:NADP$^+$ oxidoreductase E.C. 1.16.1.1) that catalyses the reduction of cytoplasmatic $Hg^{2+}_{(cyt)}$ to volatile elementary mercury $Hg^0_{(cyt)}$ (relatively inert and non-toxic for the cell, easily removable through membranar diffusion; 'cyt' notation refers to the cytosol);

– GmerD encoding the protein PmerD with a complex role (antagonist of PmerR activator function but also catalyst of *mer* operon expression even in the absence of $Hg^{2+}_{(cyt)}$ inducer). PmerD also helps PmerR in quickly repressing the PmerA expression when substrate Hg(II) is exhausted (because, like other flavin oxidoreductases in the absence of substrate, PmerA has an oxidase activity which results in production of toxic H_2O_2).

Concerning the relative concentrations of the *mer* operon expressed proteins (displayed in Table 1), the most abundant is PmerP, of optimal level around 3700 nM as for the Michaelis-Menten constant of the Hg(II) binding reaction.[1] Experimental observations indicate for the *mer* operon products the approximate ratios:[1] $[PmerP]_s = [PmerA]_s + 10 - 20$ nM, $[PmerT]_s = 0.5 \ [PmerP]_s$, $[PmerC]_s = [PmerR]_s$ (one copy-number corresponds to ca. 1 nM for an average cell volume of 10^{-15} L).[23] The stationary level (index 's') of PmerA was adopted as for PmerP, the PmerR of ca. 1000 nM (as for a protein of average level in *E. coli*),[22] while the level of PmerD was adopted much lower than those of PmerA (ca. 100 nM in Table 1) due to its secondary role of maintaining the *mer* operon expression in the absence of $Hg^{2+}_{(cyt)}$.

The *mer* gene expression, involving transcription by RNA polymerase, starts with GmerR (encoding the control gene PmerR), and then continues in the direction of structural genes GmerTPCAD. The promoter/operator regions for both structural genes GmerR and GmerTPCAD are located between genes GmerR and GmerT.[31] Expression is induced by the presence of cytosolic Hg(II) and closely regulated by the *mer* gene products itself. The whole system functions as an amplifier of expression when mercuric ions are present in significant amounts, leading to a quick (ca. 30 s) cell response and PmerRTPCAD enzyme production in cascade. In the experiment of Philippidis *et al.*[28] with cloned *E. coli* cell, the gene total concentrations are higher than normal, i.e. of ca. 3 nM. As suggested by previous work,[24,33] the stationary level of active gene has to be taken half of its total concentration for every *mer* gene (Table 1) due to the necessity to quickly control its formal catalytic activity in expression processes through rapid buffering reactions of type $G + TF \rightleftarrows GTF$. The transcription factors TF block the gene G activity through catalytically inactive GTF species. To be effective, these control reactions must be much more rapid than the catalyzed synthesis itself, while the mass conservation law must be fulfilled at all times, $[G] + [GTF] = constant$. As proved,[33] the maximum regulatory efficiency of the protein synthesis reaction at steady-state (QSS, index 's') corre-

sponds to $[G]_s/[G]_{total} = 1/2$, when the maximum regulation sensitivity vs. perturbations is reached. The allosteric control of G activity lead to successive inactive species of type $[GTF_n]$, such a schema amplifying the regulatory efficiency of the whole expression module, with a 1.3–2 multiplicative factor (usually the Performance Index P.I. concerns the recovering rate of the steady-state after a perturbation).[24] In fact, dimeric TF of proteic type are proved more effective than single molecules, in accordance to the observations of Salis and Kaznessis[34] and simulations of Maria.[22,24] Also, the control of a generic gene G expression is proved more effective in a combined self- and cross-repression schema involving intermediates of type $G(R2R2)_n(R1)_m$, where repressors are produced in the same module (R1) or in another gene expression module (R2) (the number of consecutive buffering reactions is usually $n = 1-4$, $m = 1-2$).[34]

Transport module. Hg^{2+} transport across the cellular envelope is mediated in the periplasmatic space by PmerP, and across the inner membrane by PmerT and PmerC according to a consecutive pathway schema involving P-Hg, T-Hg complexes (PmerP uses its two cysteine residues to displace the nucleophiles X to which Hg(II) is coordinated).[30–31] The membranar transport has been found to be energy-dependent and the rate-determining step for the whole mercury uptake process, i.e. several times slower than the mercury reduction (proved in separate experiments with intact and permeabilized *E. coli* cells).[28] It was also observed that membranar transport exhibits a substrate-inhibition type of kinetics, the mercury transport flux tending to reach an upper-limit at high concentrations of $[Hg^{2+}]_{env}$ ('env' notation refers to the environment). The whole transport process can be considered as being catalysed by a lumped enzyme (denoted with ET) comprising PmerP, PmerT and PmerC proteins, the stationary concentration in cytosol being calculated according to experimental observations reviewed by Barkay *et al.*:[1]

$$[ET]_s = [PmerP]_s + [PmerT]_s + [PmerC]_s \approx$$
$$\approx [PmerP]_s + 0.5\,[PmerP]_s + [PmerR]_s =$$
$$= 1.5\,[PmerP]_s + [PmerR]_s \approx \qquad (1)$$
$$\approx 1.5\,\{[PmerA]_s + 15\ nM\} + [PmerR]_s.$$

In fact, the mercury transport and reduction system is present in Gram-negative bacteria even when lacking *mer* operon, the cell being able to cope with low concentrations of mercury in the environment (below the admissible threshold in surface waters of 200 nM).[35] However, at significant pollutant loads, a specialized uptake system is less energy −intensive in getting rid of toxic metal by

reducing it to monoatomic gas (easily disposed and less toxic for the cell) than to "neutralize" it via chelate compounds (more difficult to be built and to maintain homeostasis). This specialized transport system generated by the *mer* operon via the "Hg sponge" proteins (PmerP, PmerT, PmerC, and possible PmerF, PmerE) also leads to protecting the cystein-rich proteins involved in other biochemical reactions and cell energy generation.

Once the mercuric ion complex with PmerT arrives on the inner side of the cytoplasmatic membrane, cytosolic thiol redox buffers RSH (such as glutathione), present in large excess of millimolar concentrations, compete with PmerT cytosolic cysteines to remove Hg(II) as a dithiol derivative $Hg(SR)_2$ which is substrate for PmerA enzyme.

Mercury reduction module. The agent of mercuric ion reduction in Gram-negative bacteria is the PmerA, a cytosolic flavin disulfide oxidoreductase (homodimer of 120 kDa) which uses NAD(P)H as a reductant (Fig. 1). PmerA presents a flexible amino-terminal domain, which is homologous to PmerP.[1] The overall reaction:

$$Hg^{2+}(RS^-)_2 + 2NADPH \xrightarrow{\ PmerA\ }$$
$$\xrightarrow{\ PmerA\ } Hg^0_{(cyt)} + 2NADP^+ + 2RS^- \qquad (2)$$
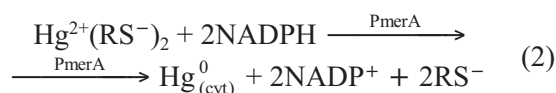
leads to production of relatively inert volatile atomic mercury $Hg^0_{(cyt)}$, which diffuses passively through the cell membranes without the need for any dedicated efflux system. As observed by Philippidis *et al.*,[28–31] an excess of NADPH usually exists in the normal *E. coli* cell with regards to the requirements of the Hg(II) reduction reaction, thus the overall kinetics being inhibited by only the substrate. The cytosolic $[NADPH]_s$ is considered in excess in the growing cell, i.e. more than 140 μM comparatively to Michaelis-Menten constant of mercuric reductase for NADPH of 13.9 μM.[28,30] A catalytic mechanism for this reaction has been proposed in the literature,[29,31] the enzyme (E) cycling between the four-electron $EH_2 \cdot NADPH$ form, to which Hg^{2+} is bound, and the two-electron form $EH_2 \cdot NADP^+$ after the release of Hg^0.

The mercuric ion transport and reduction modules can fairly represent the overall mercury uptake process and, after identification of rate constants from dynamic experiments, can be successfully used to scale-up the industrial bioprocess and for designing a bioreactor for mercury removal from polluted wastewaters.[17–19] However, such an overall model can not accurately represent the cell response to stationary or dynamic perturbations in the environment, self-regulation, *mer* gene expression amplification and cascade control, cell volume growth and inner-cell content influence to cope with pertur-

bations. This is why a structured cell model needs to be accounted for, including individual gene expression regulation but also, at a certain level of generality, the genome and proteome replication.

Cell "ballast" module. The G/P synthesis module (Fig. 1), of G(P)1 type,[23,24,36] mimics the genome (G-lump) and proteome (P-lump) replication and, due to their large concentrations, the cell content 'balast' and 'inertial' effect when coping with external/internal perturbations. The lumped proteome P plays the role of a permease for nutrients NutG, NutP import, of a metabolase for metabolites MetG and MetP synthesis, and of a polymerase for the lumped genome (G) and individual *mer*-genes synthesis. The P synthesis is assumed to be controlled by means of the simplest regulatory schema with one rapid reaction G + P $\rightleftarrows$ GP, close to its equilibrium, with dissociation constants much larger than those of the core synthesis. As investigated in previous work,[22–24] the considered G/P module in a whole-cell model tries to explicitly account for lumped interactions of individual gene expressions with the genome and proteome, and other important effects such as the cell content inertial/smoothing effect in treating perturbations, and the effect of indirect or secondary perturbations transmitted via the cell-volume under isotonic osmolarity conditions.

In the present case, the *E. coli* genome includes ca. 4500 genes (of one copy; K-12 strain; EcoCyc[37]). To allow a maximum regulatory effectiveness of the buffering reactions adjusting the genome catalytic activity, concentrations of active and inactive G-forms have been taken equal at steady-state,[22–24] i.e. $[G]_s = [GP]_s = 4500/2$ nM. The lumped proteome P concentration of $\sum_{j}^{all} c_{Pj,cyt} = 10^7$ nM was evaluated with the formula[23]

$$c_j = (\text{no. of copies of species } j)/N_A/V_{cyt,0},$$

using data for *E. coli* cell,[37–38] including ca. 1000 ribosomal proteins of $1000 - 10000$ copies, ca. 3500 non-ribosomal proteins of avg. 100 copies, and ca. 4500 polypeptides of avg. 100 copies.

The lumped metabolite species concentration of $[MetP]_s = 3 \cdot 10^8$ nM and those of external nutrients were adopted from literature.[22,25] Only the concentration of $[MetG]_s \approx 2.0017 \cdot 10^7$ nM (Table 1) resulted from fulfilment of the state-law constraint for an isotonic cell system:

$$\sum_{j}^{all} c_{j,cyt} = \sum_{j}^{all} c_{j,env}, \quad \Rightarrow \quad \sum_{j}^{all} c_{MetGj,cyt} = \sum_{j}^{all} c_{j,env} -$$

$$- \sum_{j}^{all} c_{MetPj,cyt} - \sum_{j}^{all} c_{Gj,cyt} - \sum_{j}^{all} c_{Pj,cyt}. \quad (3)$$

(where c_j = species j concentration). Concerning the mercuric ion concentrations in the environment $[Hg^{2+}]_{env}$ and cytosol $[Hg^{2+}]_{cyt}$, tested data reproduce the experiments of Philippidis *et al.,*[28] covering a large range, from traces to 120 μM.

PmerR synthesis module. The control of the *mer* gene expression is carried out by the PmerR protein, a metal-specific activator-repressor of the operon that encodes GmerR, GmerT, GmerP, GmerC, GmerA, (GmerB), and GmerD structural genes. PmerR synthesis is induced by the presence of cytosolic mercury $[Hg(RS)_2]$, acting as an amplifier of external Hg(II)-stimuli that quickly leads to activation of the *mer* operon expression over a cascade schema.[28,30–31] GmerR expression is however inhibited by high levels of $[Hg^{2+}]_{cyt}$ (see the expression module schema of Fig. 1, including a self-repression control loop via PmerR dimmers). The positive influence of other cell components on PmerR synthesis and the cell ballast effect is accounted for by means of lumped P catalytic effect. Even if PmerD is reported as being an antagonist of PmerR activator function, it is however considered here as a catalyst, present in small amounts in the cell, and maintaining a certain level of GmerR expression even when Hg(II) is absent in cytosol.[1]

Dimmers of synthesized proteins also act as TFs that regulate the gene expression by means of reversible fast buffering reactions blocking the gene catalytic activity during expression. Thus, the GmerR activity was controlled by means of a simple regulatory negative loop with one rapid buffering reaction, GmerR + PmerR::PmerR $\rightleftarrows$ GmerR::PmerRPmerR, close to its equilibrium, with dissociation constants much larger than those of the PmerR synthesis. Dimeric forms of TF, such as PmerRPmerR, have been experimentally observed,[29] leading to a reported increase in the regulatory performance indices of the expression module comparatively to monomeric TF molecules. Dimeric TF lead to a lower sensitivity to stationary perturbations and to a higher recovering rate of homeostasis after a pulse perturbation suffered by some species.[22–24] To allow a maximum regulatory effectiveness, concentrations of active and inactive GmerR forms have been taken equal at steady-state, $[GmerR]_s = [GmerRPmerRPmerR]_s = 3/2$ nM.

The dimeric TF levels for *mer*-gene expression, i.e. $[PmerRPmerR]_s$, $[PmerAPmerA]_s$ $[PmerDPmerD]_s$, and $[ETET]_s$, quickly synthesised through fast reversible reactions (Fig. 1), are optimised to confer maximum efficiency to the regulatory modules, but also to avoid an exaggerated consumption of cell energy (i.e. overshoots in the repressing/de-repressing enzyme levels).[39] A reduced TF concentration usually fulfils such requirements.

More details on the mechanistic aspect of PmerR enzyme activity are reviewed by Barkay *et al.*[1] It seems that PmerR structure establishes conditions for an instantaneous response to the presence of cytosolic Hg(II), the 'ready to rock' status in the transcriptional initiation being echoed in the NADPH-primed over-reduced EH_4 state that PmerA maintains. Moreover, the manner in which PmerR binds Hg(II) is unusual, instead of a stable/long-term bond, PmerR develops a strong but transient relationship with the metallic ions.

ET, PmerA, and PmerD synthesis modules. The synthesis of the lumped ET transport enzyme (summing PmerP, PmerT, and PmerC), is modelled through a lumped gene GT expression (summing GmerP, GmerT, and GmerC; Fig. 1). The catalytic role of proteome P is included together with the activation role of PmerR control protein. Similar to the PmerR, ETET dimmers also play the role of TF that self-regulate the expression by means of reversible fast buffering reactions blocking GT activity. Due to the previously mentioned reasons, at steady-state $[GT]_s = [GT::ETET]_s = 3/2$ nM.

Similar gene expression modules are constructed for synthesis of PmerA and PmerD, with the same self-control of the expression level using dimeric TF (Fig. 1). The steady-state levels of active/inactive G-forms are: $[GmerA]_s = [GmerAPmerAPmerA]_s = 3/2$ nM, $[GmerD]_s = [GmerDPmerDPmerD]_s = 3/2$ nM. Once PmerR is produced, the cross- and self-control lead to GmerA and GmerD expression. The PmerD role of assisting PmerR to quickly repress PmerA expression when substrate Hg(II) is exhausted was not accounted in the present model. It was considered that the adopted Hill-type amplifier/decelerator kinetics for PmerR synthesis/decline, with a multiple control exerted by P, PmerD, and PmerR could satisfactorily account for such a quick response (see below section on the amplifier effect).

In the present model, the expression of GT, GmerA, and GmerD is made simultaneously in separate regulatory modules once PmerR is produced quantitatively. Further model developments can easily account for a consecutive synthesis schema, in which expression of GmerD follows those of GmerA and GT, by accounting as catalyst (beside PmerR) the ET for GmerA expression, and of PmerA for GmerD expression. The present approach will however not affect the cell homeostasis (stationary species levels of GmerA/PmerA and GmerD/PmerD) or the recovering rates after a perturbation, but will only ignore the small delay existing between 'time windows' of species PmerA and PmerD transition.

Finally, it is noteworthy that, according to remarks of Barkay *et al.*,[1] despite being the longest studied bacterial toxic metal resistance loci, the *mer* operon continues to bring new insights into gene regulation and involved enzymatic metabolic processes of the bacteria, as long as significant parts of the process control mechanism remain yet unknown.

Kinetic model for the mercury reduction and the GRC pathway

The proposed kinetic model for mercuric ion reduction accounts for 33 reactions (Table 3), corresponding to the reaction pathway of Fig. 1. The process mechanism involves seven regulatory modules aiming at controlling the mercury transport and reduction but also the *mer* operon expression in connection to the whole cell content replication during the cell cycle. The whole-cell approach becomes functional when maintaining homeostasis of *E. coli* cell under equilibrated growth conditions. To better represent the GRC properties, the model includes information on the key-intermediates and elementary steps in connection with the rest of the lumped cell content evolution, with a degree of detail depending on the available information and desired model extension. In such a manner, by placing the regulatory module chain in a growing cell, the whole content behaviour can be mimicked under simulated stationary or perturbed environmental conditions.

The reactions are considered elementary, with first or second order kinetic expressions (Table 3). Exceptions concern the mercury transport and reduction steps for which consistent data are reported, and also the GmerR transcription initiation and control for which analogies with fast inducible GRC from literature (working in certain conditions as an amplifier) may be used. Both mercuric ion mediated membranar transport and enzymatic reduction in cytosol are extensively experimentally studied by Philippidis *et al.*[28–31]

Separate experiments with intact and permeabilized *E. coli* cell prove that mercuric ion membranar import from environment is the rate limiting step, the rate expression being of Michaelis-Menten type with substrate $Hg_{(env)}^{2+}$ inhibition and catalysed by ET lumped enzyme. The cytosolic thiol redox buffers *RSH* being present in large excess for coupling the cytosolic Hg(II) as dithiol derivative $Hg(SR)_2$, the rate expression becomes:

$$Hg_{(env)}^{2+} + 2RSH \xrightarrow{ET} Hg(SR)_2 + 2H^+;$$

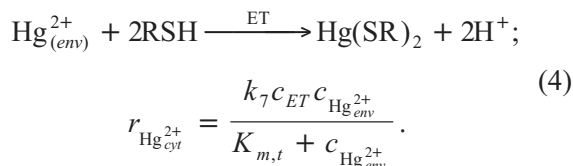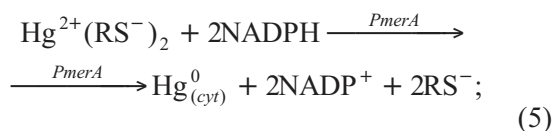$$r_{Hg_{cyt}^{2+}} = \frac{k_7 c_{ET} c_{Hg_{env}^{2+}}}{K_{m,t} + c_{Hg_{env}^{2+}}}. \tag{4}$$

T a b l e 3 – *Kinetic parameters of the whole-cell model identified for stationary E. coli cell conditions and overall mercury reduction rate of Philippidis et al.[28,30–31] (E. coli cell with plasmid R100 as source of mer operon; $[TF]_s = 4$ nM; the symbol '~' indicate approximate values to avoid displaying 16-digits mantissa numbers; reaction rates are in nM min^{-1} referred to the cell volume).*

Reaction	Rate expression, $\dfrac{1}{V}\dfrac{dn_j}{dt}$	Rate constants (units correspond to min and nM)
$NutG + P \rightarrow MetG + P$	$k_1[NutG][P]$	$3.3376 \cdot 10^{-10}$
$NutP + P \rightarrow MetP + P$	$k_2[NutP][P]$	$5.1678 \cdot 10^{-10}$
$MetG + P \rightarrow G + P$	$k_3[MetG][P]$	$1.1242 \cdot 10^{-13}$
$MetP + G \rightarrow P + G$	$k_4[MetP][G]$	$7.4106 \cdot 10^{-8}$
$G + P \rightarrow GP$	$k_5[G][P]$	$\sim 1.0 \cdot 10^{-2}$
$GP \rightarrow G + P$	$k_6[GP]$	10^5 (adopted)
$Hg^{2+}_{(env)} + ET + (2RSH) \rightarrow Hg^{2+}_{(cyt)} + ET + (2H^+)$	$\dfrac{k_7[ET][Hg^{2+}]_{env}}{K_{m,1}+[Hg^{2+}]_{env}}$ $k_7[ET] = r_{max,t}$	$K_{m,1} = 3800$ nM $r_{max,t} = 8.2 \cdot 10^6$ nM min^{-1} $k_7 = 1.2476 \cdot 10^3$ min^{-1}
$Hg^{2+}_{(cyt)} + PmerA + (2NADPH) \rightarrow$ $Hg^0_{(cyt)} + PmerA + (2NADP^+ + 2RSH)$	$\dfrac{k_8[PmerA][Hg^{2+}]_{cyt}}{K_{m,P}+[Hg^{2+}]_{cyt}+[Hg^{2+}]^2_{cyt}/K_{i,P}}$ $k_8[PmerA] = r_{max,P}$	$K_{m,P} = 1.26 \cdot 10^4$ nM $K_{i,P} = 9.67 \cdot 10^4$ nM $r_{max,P} = 45 \cdot 10^6$ nM min^{-1} $k_8 = 9.5305 \cdot 10^3$ min^{-1}
$Hg^0_{(cyt)} \rightarrow Hg^0_{(env)}$	$k_9[Hg^0]_{cyt}$	$2.1832 \cdot 10^3$
$MetG + (P + Hg^{2+}_{(cyt)} + PmerD + PmerR) \rightarrow GmerR$	$\dfrac{k_{10}[PmerD][MetG][P](1+b[Hg^{2+}]^4_{cyt})}{(K_{GmerR}+[[Hg^{2+}]^4_{cyt})[PmerR]^{0.5}}$	$K_{GmerR} = 1.3841 \cdot 10^{14}$ nM^4 $k_{10} = 3.3857 \cdot 10^{-7}$ min^{-1} nM$^{-1.5}$ $b = 1.4 \cdot 10^{-10}$ nM^{-4}
$MetG + GmerR \rightarrow PmerR + GmerR$	$k_{11}[MetP][GmerR]$	$1.1235 \cdot 10^{-8}$
$GmerR + PmerRPmerR \rightarrow GmerRPmerRPmerR$	$k_{12}[GmerR][PmerRPmerR]$	$\sim 2.5 \cdot 10^4$
$GmerRPmerRPmerR \rightarrow GmerR + PmerRPmerR$	$k_{13}[GmerRPmerRPmerR]$	10^5 (adopted)
$2PmerR \rightarrow PmeRPmerR$	$k_{14}[PmerR]^2$	$\sim 4 \cdot 10^{-1}$
$PmerRPmerR \rightarrow 2PmerR$	$k_{15}[PmerRPmerR]$	10^5 (adopted)
$MetG + (P + PmerR) \rightarrow GT + (P + PmerR)$	$k_{16}[MetG][P][PmerR]$	$7.4951 \cdot 10^{-20}$
$MetP + GT \rightarrow ET + GT$	$k_{17}[MetP][GT]$	$7.3165 \cdot 10^{-8}$
$GT + ETET \rightarrow GTETET$	$k_{18}[GT][ETET]$	$\sim 2.5 \cdot 10^4$
$GTETET \rightarrow GT + ETET$	$k_{19}[GTETET]$	10^5 (adopted)
$2ET \rightarrow ETET$	$k_{20}[ET]^2$	$\sim 9.26 \cdot 10^{-3}$
$ETET \rightarrow 2ET$	$k_{21}[ETET]$	10^5 (adopted)
$MetG + (P + PmerR) \rightarrow GmerA + (P + PmerR)$	$k_{22}[MetG][P][PmerR]$	$7.4951 \cdot 10^{-20}$
$MetP + GmerA \rightarrow PmerA + GmerA$	$k_{23}[MetP][GmerA]$	$4.1242 \cdot 10^{-8}$
$GmerA + PmerAPmerA \rightarrow GmerAPmerAPmerA$	$k_{24}[GmerA][PmerAPmerA]$	$\sim 2.5 \cdot 10^4$
$GmerAPmerAPmerA \rightarrow GmerA + PmerAPmerA$	$k_{25}[GmerAPmerAPmerA]$	10^5 (adopted)
$2PmerA \rightarrow PmerAPmerA$	$k_{26}[PmerA]^2$	$\sim 2.92 \cdot 10^{-2}$
$PmerAPmerA \rightarrow 2PmerA$	$k_{27}[PmerAPmerA]$	10^5 (adopted)
$MetG + (P + PmerR) \rightarrow GmerD + (P + PmerR)$	$k_{28}[MetG][P][PmerR]$	$7.4951 \cdot 10^{-20}$
$MetP + GmerD \rightarrow PmerD + GmerD$	$k_{29}[MetP][GmerD]$	$1.2335 \cdot 10^{-9}$
$GmerD + PmerDPmerD \rightarrow GmerDPmerDPmerD$	$k_{30}[GmerD][PmerDPmerD]$	$\sim 2.5 \cdot 10^4$
$GmerDPmerDPmerD \rightarrow GmerD + PmerDPmerD$	$k_{31}[GmerDPmerDPmerD]$	10^5 (adopted)
$2PmerD \rightarrow PmerDPmerD$	$k_{32}[PmerD]^2$	$\sim 4 \cdot 10^1$
$PmerDPmerD \rightarrow 2PmerD$	$k_{33}[PmerDPmerD]$	10^5 (adopted)

Rate parameters $r_{\max,t} = k_7[ET]$ and $K_{m,t}$, presented in Table 3, are those identified by Philippidis *et al.*[28–31] from kinetic data using intact *E. coli* cells [referred to the cell volume, for a biomass density of $\rho_X = 10^6$ mg (L cell)$^{-1}$], while k_7 was identified from $[Hg^{2+}]_{env} = 40$ μM data. More detailed rate expressions are also proposed, but lacking accurate sets for certain parameters such as membrane effective permeability, membrane area per cell volume, or dissociation constants.

The Hg^{2+} reduction in cytosol to Hg^0, has been considered with a kinetics of modified Haldane type, with substrate inhibition:[19,28,30–31]

$$\mathrm{Hg}^{2+}(\mathrm{RS}^-)_2 + 2\mathrm{NADPH} \xrightarrow{\quad PmerA \quad}$$
$$\xrightarrow{\quad PmerA \quad} \mathrm{Hg}^0_{(cyt)} + 2\mathrm{NADP}^+ + 2\mathrm{RS}^-; \tag{5}$$

$$r_{\mathrm{Hg}^0_{cyt}} = \frac{k_8 c_{PmerA} c_{\mathrm{Hg}^{2+}_{cyt}}}{K_{m,P} + c_{\mathrm{Hg}^{2+}_{cyt}} + c^2_{\mathrm{Hg}^{2+}_{cyt}}/K_{i,P}}.$$

Rate parameters $r_{\max,P} = k_8[PmerA]$, $K_{m,P}$ and $K_{i,P}$, presented in Table 3, are those identified by Philippidis *et al.*[28–31] from kinetic data using permeabilized *E. coli* cells for which membranar transport resistance is eliminated. The k_8 was identified from $[Hg^{2+}]_{env} = 40$ μM data. More detailed rate expressions are also proposed in literature, accounting for the NADPH role in complex intermediates. However, the resulted competitive inhibition of a hyperbolic model type with seven inhibition terms is difficult to fit from data. As a large excess of NADPH exists in the growing *E. coli* cell (millimole concentrations comparatively to micromole cytosolic mercury), the reduced kinetics can fairly represent the reduction process dynamics.

Initiation of the *mer* operon expression at low concentrations of $[Hg^{2+}]_{cyt}$ inducer (even at nanomolar levels), involves a quick PmerR synthesis. The resulted PmerR protein will then initiate and catalyse the synthesis of other proteins involved in the mercuric ion reduction process, over a cross- and self- control scheme in cascade. Due to such a role played by GmerR expression, amplifying the external stimuli and quickly triggering the suitable enzyme synthesis, the Hill-type activation kinetics has been adopted:[22,40]

$$r_{GmerR} = \frac{k_{10} c_{MetG} c_P c_{PmerD}\left(1 + b\, c^4_{\mathrm{Hg}^{2+}_{cyt}}\right)}{\left(K_{GmerR} + c^4_{\mathrm{Hg}^{2+}_{cyt}}\right)\sqrt{c_{PmerR}}}. \tag{6}$$

Such kinetics account for four molecules of inducer Hg(RS)$_2$, allosterically binding the promoter site, while a slow self-repression with the product PmerR is accounted with an usual -0.5 apparent

reaction order.[40] PmerD enzyme plays the role of an activator, allowing to maintain a low level of expression even in the absence of the inducer.[1] The rate constant $K_{GmerR} = c^4_{\mathrm{Hg}^{2+}_{cyt},ref} = (3430)^4$ (nM^4, referring to the cell volume) was adopted at the optimum value of Hill-type inducible GRC of $[\ln]^n = [\mathrm{Hg}^{2+}]^4_{s,cyt}$. The adopted constant $b = 1.4 \cdot 10^{-10}$ (nM^{-4}) follows the specifications of Voit[40] for a general genetic amplifier of Hill type. Thus, in the kinetics term $(1 + b\, c^4_{In})$, typical b value is $b = 2$ (nM^{-4}) for an inducer concentration of $c_{In} = 0 - 10$ (nM), which corresponds to $b = 1.4 \cdot 10^{-10}$ (nM^{-4}) for a cytosolic mercury average concentration of $c_{\mathrm{Hg}^{2+}_{cyt}} = 3430$ (nM) in the present case. It is also to observe that GmerR expression amplifier role exists only at low and moderate concentrations of mercury in the environment, while high pollutant levels (larger than $30-40$ μM) lead to high cytosolic concentrations of $[Hg^{2+}]$ and inhibition of the GmerR expression.

After convenient parameterisation, the rate constants of the model have been identified from solving the stationary mass balance equations with substituted concentrations of observable species corresponding to a nominal steady-state, by also accounting for the cell-volume growth due to variation of species copynumbers during metabolic reactions under isotonic osmolarity. Then, the remaining unknowns of the model were fitted to match the stationary overall reduction rate of Hg^{2+} recorded from experiments carried out in chemostat cultures, and repeated at various environmental $[Hg^{2+}]_{env}$ levels (experiments with *E. coli* and plasmid R100 as source of *mer*-operon of Philippidis *et al.,*[28,30–31] see also Leonhäuser *et al.*[19]). However, lacking stationary data for some cytosolic species and conventional kinetic data for species evolution over transient regimes (difficult to be obtained experimentally), supplementary degrees of freedom are still available in the dynamic model. This well-known low estimability is solved by using any type of information on dynamic system properties.[54,22] In this paper, several levels of information are used in the analysis: i) check the Michaelis-Menten constants for the mercuric ion membranar transport and reduction (eq. 4–5), from separate experiments performed by Philippidis *et al.*[28] using intact or permeabilized *E. coli* cells; ii) check the model validity in other steady-state conditions than those used in identification (by using Philippidis *et al.*[28] data); iii) adjust the GRC model holistic properties, by minimizing the recovering times of the homeostasis after a dynamic perturbation (i.e. minimum AVG), or inner species level sensitivity to external perturbations (see the review of Maria[22–23] for other
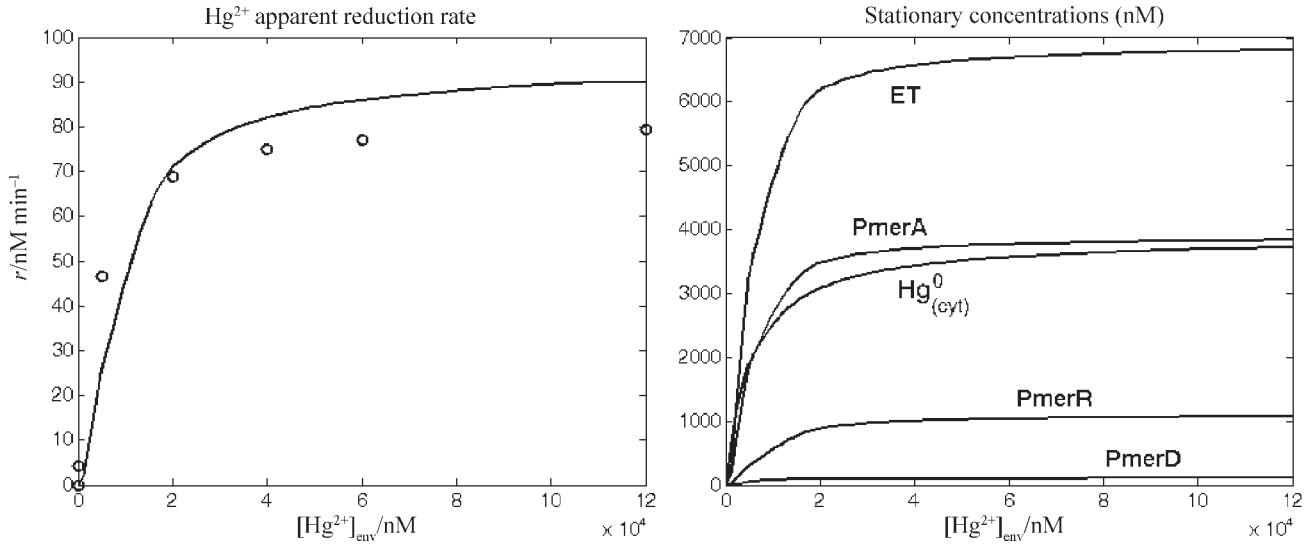
F i g . 2 – *(Left) Experimental (o)[28] and predicted (–) values of the apparent reduction rate of mercuric ions on E. coli cell by using the identified whole-cell model (with [TF]$_s$ = 4 nM) for various environmental Hg^{2+} stationary concentrations. (Right) Stationary concentrations (at homeostasis) of the main involved species in the mer-operon expression pathway for various environmental conditions.*

GRC properties); iv) minimize the level of reaction intermediates (including TF) used in the GRC schema, in order to minimize the cell resource consumption (metabolites and chemical energy). Unobservable variables, such as stationary concentration of ET, PmerR, PmerA, PmerD, or optimum TF levels can thus be adjusted accordingly. Exceptions are the dissociation constants of the buffer reactions that control the gene activity via fast reversible bonds with dimeric TF, adopted much faster than other cell processes, i.e. 10^5 min^{-1} (Table 3).[22–24,36] The identified rate constants are presented in Table 3, using the experimental data of Philippidis *et al.*[28] (Fig. 2, left), at environmental mercuric ion levels ranging from 5 to 120 μM (and 1 mM NADPH). An adopted dimmer concentration of [TF]$_s$ = 4 nM for all gene expressions has been found adequate. Higher stationary TF levels can still improve regulatory P.I. of modules but with the expense of a higher cell energy consumption.

In all the simulated cases, the cell system results as stable, with a stable homeostasis. In mathematical terms, this constraint has been fulfilled by calculating the real parts of the eigenvalues λ_j of the model function Jacobian and imposing (through the fitted [TF]$_s$) that all be negative, $Re(\lambda_j) < 0$.

Whole-cell model under variable volume framework

Variable volume cell modelling has been introduced by Grainger,[41–42] exemplified and discussed in a whole-cell approach by Morgan *et al.*[25] and Maria,[22–24] and applied by Tomita *et al.*[43–44] and Kinoshita *et al.*[26] to develop extensive cell simula-

tion platforms for *Mycoplasma genitalium*. In fact, the VVWC modelling framework is based on the mass balance equations written in terms of concentrations for a variable-volume system,[45] but completed with system invariants derived for isotonic diluted solutions (Pfeffer's law),[46] and reaction invariants:

$$\frac{dc_j}{dt} = \frac{1}{V}\frac{dn_j}{dt} - D\,c_j = g_j(\boldsymbol{c},\boldsymbol{k});$$

(at steady-state: $g_j(\boldsymbol{c_s},\boldsymbol{k}) = 0$);

$$\frac{1}{V}\frac{dn_j}{dt} = r_j(\boldsymbol{c},\boldsymbol{k}); \quad j = 1,\ldots,n_s;$$

Pfeffer's law: $\pi V(t) = RT\sum_{j=1}^{n_s} n_j(t);$

$$D = \frac{1}{V}\frac{dV}{dt} = \left(\frac{RT}{\pi}\right)\sum_{j=1}^{n_s}\left(\frac{1}{V}\frac{dn_j}{dt}\right);$$

$$\pi_{cyt} = \pi_{env} = \text{constant}, \qquad (7)$$

$$\Rightarrow \left(\sum_j^{all} c_j\right)_{cyt} = \left(\sum_j^{all} c_j\right)_{env}.$$

(where: V = cell volume; c_j = species j concentration; n_j = species j number of moles; D = cell-content dilution rate; π = osmotic pressure; T = temperature; R = universal gas constant; n_s = number of species inside the cell; t = time). The isotonic cell system assumption, made for the growing phase of the cell (ca. 80 % of the cell-cycle), leads

to fulfillment of the following invariance relationship:

$$\frac{RT}{\pi} = \frac{V}{\sum_{j=1}^{n_s} n_j} = \frac{1}{\sum_{j=1}^{n_s} c_j} = \frac{1}{\sum_{j=1}^{n_s} c_{j0}} = \text{constant}, \quad (8)$$

which implies that perturbations in species and reaction rates will influence the volume growth, which in turn will perturb the other cell component concentrations by means of the so-called 'secondary perturbations' transmitted through the common cell volume. Thus, in a VVWC modelling approach cell species connections appear due to common reactions, or common intermediates participating in chain reactions, but also indirectly via the cell-volume to which growth all components contribute.[23] Due to the state law constraint, in a VVWC model all species have to be represented individually or included as lumps, and every process has to be included at some level of detail. Thus, the rates of individual reactions within cell are constrained by the periodicity of the cell-cycle (t_c) and by the requirement that mole amounts of all components and the volume must double in exactly one cell-cycle. The main VVWC modelling hypotheses are presented by Maria,[22] and they correspond to an open system of uniform content, with a semi-permeable membrane of negligible volume and resistance to species diffusion, and to a constant osmotic pressure ensuring the membrane integrity. The logarithmic growing rate of average $D_s = \ln 2/t_c$ corresponds to a uniform exponential volume growth of $V = V_0 \exp(D_s t)$.

The VVWC modelling framework presents various advantages, but also some drawbacks related to the increased model complexity and requirement to include information not only on the studied metabolic pathway but also on all key species (even treated as lumps) and holistic properties. In spite of its increased complexity vs. classical/default constant volume modelling framework, the VVWC approach can fairly represent complex cell processes such as GRC. By explicitly linking the volume growth, external conditions, osmotic pressure, cell content ballast and net reaction rates for all cell-components, prediction of local and holistic properties of the metabolic network becomes possible.[22–25]

By placing the regulatory module chains in a growing cell, the whole content behaviour can be mimicked under simulated stationary or perturbed environmental conditions. As proved by Morgan *et al.*[25] and Maria,[22–23] the large cell-'ballast' tends to stabilize the system and to smooth perturbations in key species levels, thus decreasing the GRC responsiveness. The VVWC modelling approach leads to tighter species/reaction interconnectivity under isotonic conditions. When modelling a GRC, characterization of the individual gene expression regulatory module efficiency is connected to the imposed holistic properties of the whole cell construction.[22] For instance, a VVWC with a large content lead to smoothed perturbations of stationary concentration levels but to longer transient times in comparison to a cell with a 'sparing' content. Also, optimized P.I. of a GRC can result significantly different compared to the classical approach. For instance, the recovering rates of species present in small amounts, after a dynamic perturbation, resulted smaller in a VVWC formulation due to supplementary imposed constraints and a synchronized response of the cell system.[22]

For a GRC, various P.I. of regulatory loops can be defined and used to analyse the individual regulatory modules for gene expression or other catalytic reactions. Identifiable GRC functions can be thus pointed-out and regulatory properties quantitatively studied in connection to certain types of regulatory units. For instance, a linear dependence between a regulatory unit P.I. and the number of the allosteric control steps can be easily established for every TF type.[23–24,36] Regulatory P.I. have been extensively discussed in the literature, and new ones have been proposed to better characterize a GRC under VVWC framework.[22–24,47–49] The present work is focused on the following P.I. used to characterize the effectiveness of the modular regulatory network:

i) *Stationary efficiency* is defined by means of the sensitivity coefficient $s(c_j; c_i) = (\partial c_j / \partial c_i)_s$, i.e. the species j quasi-steady-state sensitivity vs. stationary perturbations in species i level (internal or external). The cell species sensitivities are evaluated following the Maria[23] rule by differentiating the model (7) equations. If these sensitivities are normalized referring to a stationary state (index 's'), the relative sensitivities can also be obtained $S(c_j; c_i) = (\partial \ln(c_j)/\partial \ln(c_i))_s$.

ii) *Responsiveness* to exo- or endogeneous signalling species, can be represented by the small transient times τ_j necessary to a species j stationary level to reach a new steady-state (with a certain tolerance) after application of a stationary external stimulus. Such a P.I. must be accompanied by the requirement that overshoots in the level of enzymes repressing or de-repressing the gene expression to be tolerable.

iii) *Dynamic efficiency* represented by the species j fast recovering time ($\tau_{rec,j}$) of the steady-state, with a tolerance of 5 %[47] or 1 %,[23] after an impulse-like perturbation.

iv) *Overall responsiveness* of the modular GRC, approximated by the average transient time $AVG(\tau_j)$ of species.[23]

v) *Species connectivity* can be also viewed as a measure of response synchronisation when coping with perturbations during transition time-intervals. A global connectivity P.I. was proposed as being the standard deviation $STD(\tau_j)$ of transient time of species.[23]

vi) *System stability, stability region and strength*. By writing the model in the general form, $dc/dt = g(c, k, t)$, and by using the quasi-linearization around the steady-state, $dc/dt \approx J^T c$ (where $J = dg/dc$ is the system Jacobian matrix), one can check the QSS stability from the condition that $Re(\lambda_j) < 0$ for all j, where λ_j are the eigenvalues of the J matrix evaluated at the steady-state. Supplementary checks includes the local stability,[50] conditions of oscillations,[51] and the sufficient conditions for bifurcation $[tr(J) = 0, tr(\partial J/\partial k) \neq 0]$.[52] Stability region and strength can also be characterized in mathematical terms following the rules of Hlavacek and Savageau,[47] and Maria.[23]

Predictive functions of the whole cell-model

Prediction of cell response to dynamic (impulse-like) perturbations

After identification of the proposed VVWC model for mercuric ion reduction in *E. coli* cell, by using the experimental data of Philippidis *et al.*,[28,30–31] checking the involved GRC properties is necessary in order to characterize and adjust the regulatory network efficiency by means of some species levels (usually TF).

To study the cell response to dynamic (impulse-like) perturbations, one perturbs the stationary concentration of one key-species for the mercury reduction process (e.g. PmerR) by a diminishment with 10 % (instantaneously), and calculates the recovering times of steady states (homeostasis) for all cell species ($\tau_{rec,j}$, with 1 % tolerance). The results are presented in Fig. 3 (up) for $[TF]_s = 1$ nM. By calculating the mean $AVG(\tau_{rec,j})$, and the standard deviation of the recovering times $STD(\tau_{rec,j})$, one can evaluate the overall species degree of connectivity and synchronization when gene expression is coping with a perturbation. Simulations performed at stationary $[Hg^{2+}]_{s,env} = 40$ μM, indicate an AVG = 164.17 min, and a STD = 197.59 min. As expected, the recovering times of species present in large amounts are negligible (MetG, MetP, P, G, GP, $Hg^{2+}_{(cyt)}$, $Hg^0_{(cyt)}$), while those of species displaying small concentrations are significant (ca. 100–200 min for those belonging to the GmerR/PmerR module, and ca. 200–400 min for those related to other gene expression modules).

Even if recovering times for some species are larger than the cell cycle (139 min), it was proved that such a situation is not uncommon. As observed by Elowitz and Leibler,[53] the transition times in the inductive/co-repressed GRC systems can be much larger than the cell-division cycle, the state of the oscillator, transient switch or amplifier being transmitted from generation to generation.

It is expected that species recovering times $\tau_{rec,j}$, and their steady-state sensitivity to environmental species, e.g. $(\partial \ln(c_j)/\partial \ln[Hg^{2+}]_{env})_s$, be controlled by the level of some intermediates.[22] Indeed, by simulating the recovering scenarios for various $[TF]_s$, the resulted P.I. are better with the increase of $[TF]_s$ from 0.1 to 6 nM, i.e. smaller $\tau_{rec,j}$ (plotted in Fig. 3-down) and sensitivities to environmental changes (not presented here). In a previous work, studying genetic bistable switches behaviour, Maria[22] found that large TF levels tends to increase the stability strength of the GRC system, which in mathematical terms corresponds to smaller $Re(\lambda_j)$. In the mercury reduction case, the GRC presents only one steady-state which is stable for large ranges of $[TF]_s$. However, the stability strength predicted by this model seems to be slightly better for small $[TF]_s = 0.1$ nM, with $Max|Re(\lambda(J))| = 1.7 \cdot 10^6$, than those for large $[TF]_s = 6$ nM, with $Max|Re(\lambda(J))| = 2.4 \cdot 10^5$. A reasonable level of $[TF]_s = 4$ nM should be further considered in the model, larger overshoots of these intermediate species being energetically unfavourable. The adjustable levels of $[TF]_s$ can be used to control the GRC properties and, indirectly, the overshoots in the level of enzymes repressing or de-repressing the gene expression.

As another observation, the present model includes both self- and cross-repression of every gene expression from the *mer* operon, in accordance with the reported results. As proved by Salis and Kaznessis[34] and Maria,[22] such a mixed repression allows better control of the expression, of a higher flexibility, by decreasing the over-expressed protein levels, and by reducing the transient and recovering times after perturbations in the environment.[47]

Prediction of cell response to stationary (step-like) perturbations

To study the cell response to stationary (step-like) perturbations of the environmental conditions, one perturbs the stationary $[Hg^{2+}]_{s,env}$ by instantaneously increasing its level from 40 μM to 50 μM. The simulated species transient times τ_j, necessary to reach the new steady-state (with 1 % tolerance), are presented in Fig. 4 (up) for $[TF]_s = 1$ nM. The resulted overall regulatory
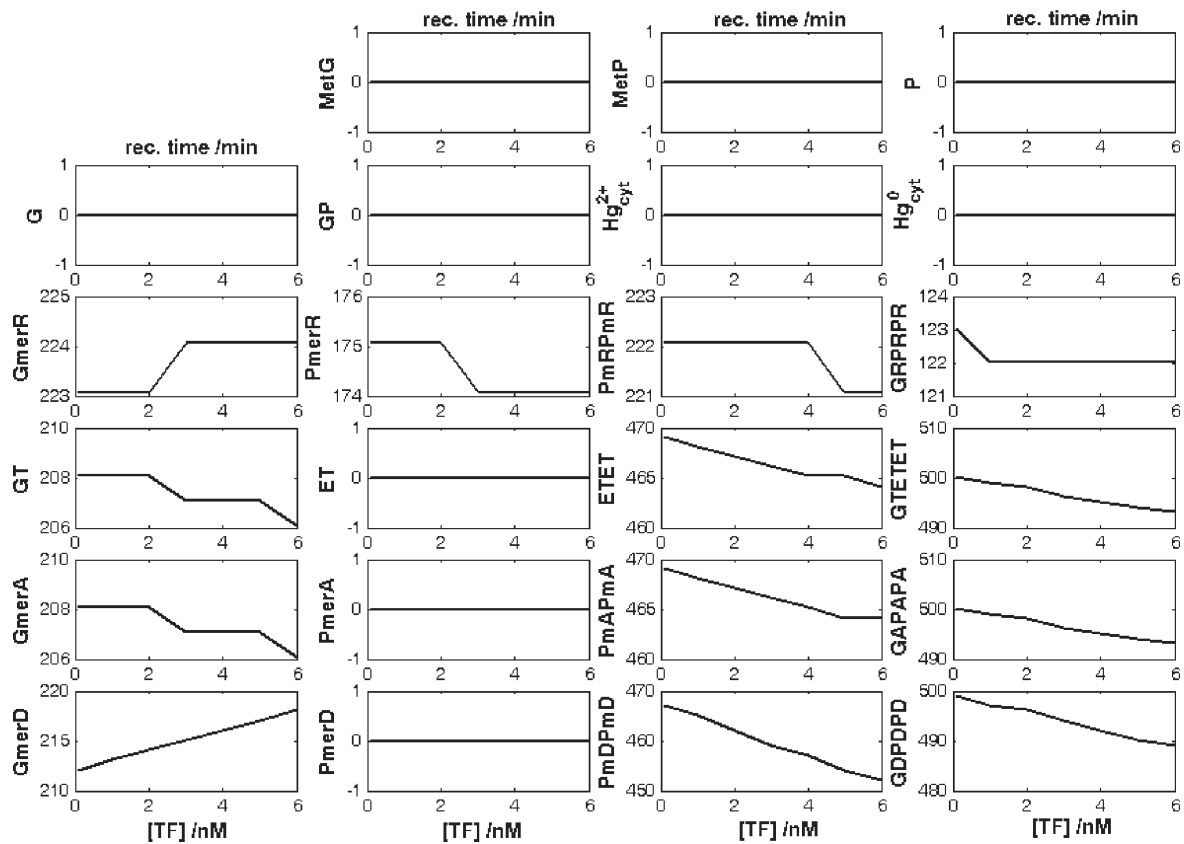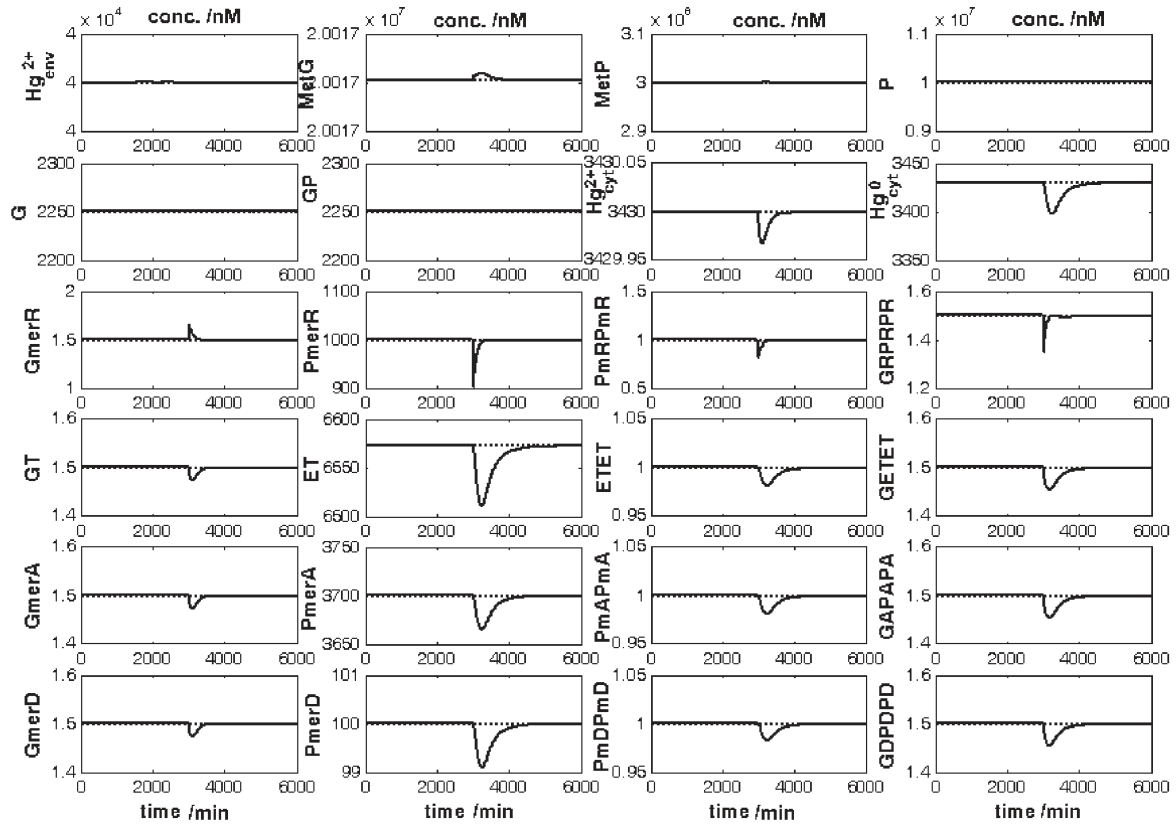
F i g . 3 – *Species recovering times to QSS ($\tau_{rec,j}$, with 1 % tolerance), predicted by the cell-model, after a −10 % $c_{PmerR,s}$ impulse perturbation, in the presence of a stationary external stimulus $[Hg^{2+}]_{s,env} = 40\ \mu M$. (Up) Results for TF = 1 nM (i.e. PmerRPmerR, ETET, PmerAPmerA), leading to AVG = 164.17 min, and STD = 197.59 min (recovering times of species MetG, MetP, P, G, GP, $Hg^{2+}_{(cyt)}$, $Hg^{0}_{(cyt)}$ are less than 1 min). (Down) Predictions of $\tau_{rec,j}$ for various $[TF]_s$. AVG varies from 164.5 min ($[TF]_s = 0.1$ nM) to 162.5 min ($[TF]_s = 6$ nM). STD varies from 198.1 min ($[TF]_s = 0.1$ nM) to 194.9 min ($[TF]_s = 6$ nM).*

Paper prepared for the special issue of Chem. & Biochemical Eng. Quarterly, 2007
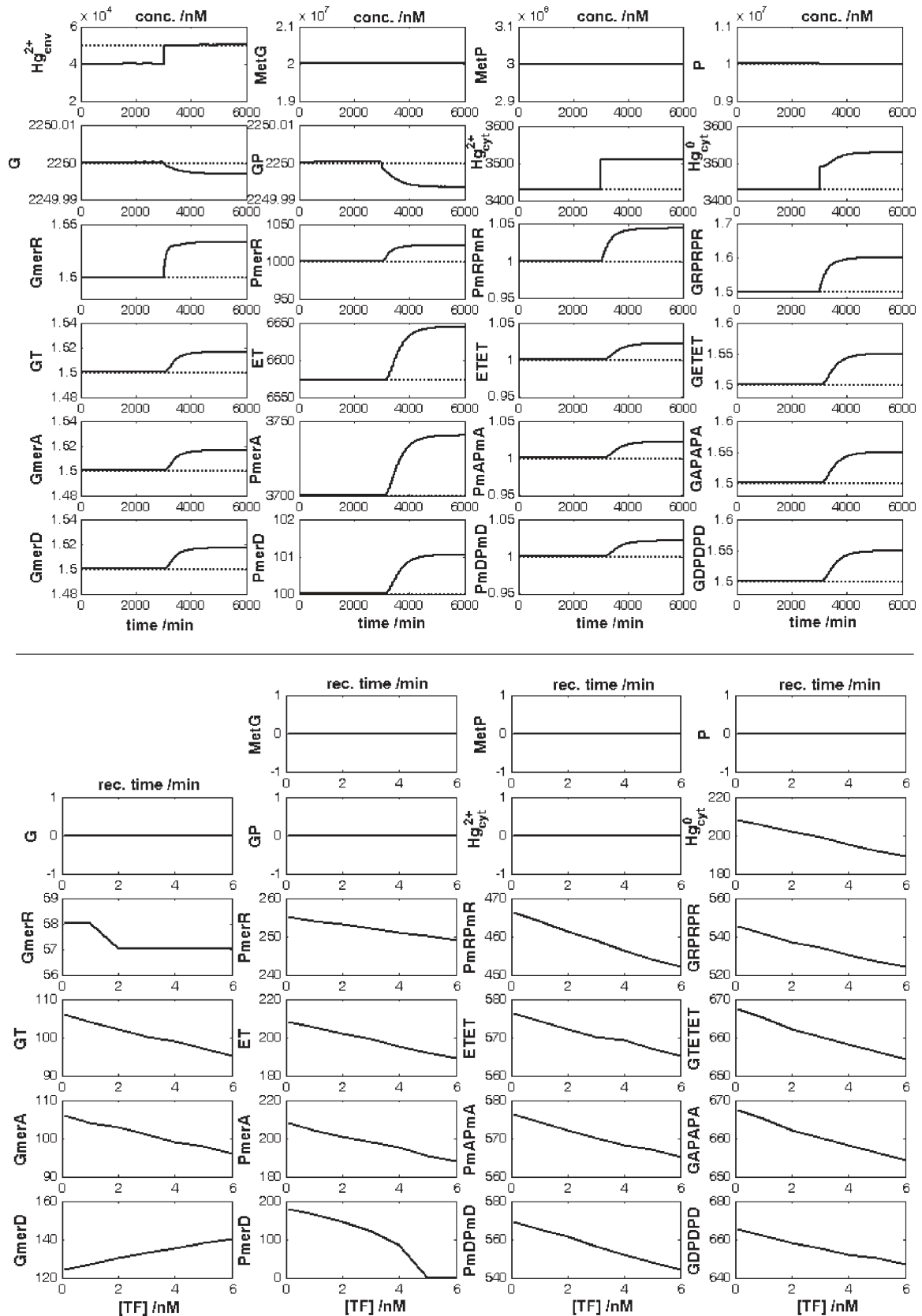

F i g .   4 – *Species transient times τ_j (with 1 % tolerance), predicted by the cell-model, after a step-perturbation in the environmental mercury from $[Hg^{2+}]_{s,env} = 40\ \mu M$ to $[Hg^{2+}]_{s,env} = 50\ \mu M$. (Up) Results for $[TF] = 1\ nM$ (i.e. PmerRPmerR, ETET, PmerAPmerA), leading to AVG = 236.0 min, and STD = 254.6 min (transition times of species MetG, MetP, P, G, GP, $Hg^{2+}_{(cyt)}$, $Hg^{0}_{(cyt)}$ are less than 1 min). (Down) Predictions of τ_j for various $[TF]_s$. AVG varies from 237.8 min ($[TF]_s = 0.1\ nM$) to 223.4 min ($[TF]_s = 6\ nM$). STD varies from 255.5 min ($[TF]_s = 0.1\ nM$) to 253.0 min ($[TF]_s = 6\ nM$).*

efficiency indices are AVG = 236.0 min, and STD = 254.6 min, indicating transient times smaller for G•/P• pairs (ca. 100-200 min) but larger for intermediates of P•P• or G•P• P• type (400−500 min). Such a result can be explained by the role of intermediates in smoothing the perturbations on each gene expression module, but also in synchronizing the cell key component response with paying the price of a longer transition.

To study the influence of the TF levels on the species transient times $\tau_{rec,j}$ and their steady-state sensitivity to environmental conditions $(\partial \ln(c_j)/\partial \ln[\mathrm{Hg}^{2+}]_{env})_s$, repeated simulations of step perturbations are performed. The results, plotted in Fig. 4 (down), lead to similar conclusions as for impulse-like perturbation case, that is the *mer*-operon expression regulatory efficiency increases with the TF level. Thus, AVG ($\tau_{rec,j}$) declines from 238 min to 223 min for an increase of [TF]$_s$ from 0.1 to 6 nM (with a practically unchanged STD), and as the relative sensitivities to environmental changes (not presented here).

Amplification effect of mer-operon expression at low levels of cytosolic Hg(II)

The main function of the GmerR expression module is to rapidly induce and control the expression of the *mer* operon when concentrations of ionic mercury become significant. Indeed, it is experimentally observed that, in ca. 30 s the *E. coli* cell responds vigorously to such perturbations even for sub-micromolar [Hg^{2+}]$_{env}$ concentrations.[1] This behaviour suggests a Hill-type induction of the GmerR expression, playing the role of an amplifier of the external stimuli leading to speed-up the *mer* gene expression. To study the amplification effect when large copynumbers of *mer* genes are present, Philippidis et al.[28] cloned *E. coli* cell with an increasing number of plasmid vectors ranging from 3 to 140 copies per cell.

To verify the model capabilities to reproduce such an effect, simulations of stationary reduction of Hg^{2+} have been performed for different environmental mercuric ion concentrations, ranging from 0.2 to 120 μM, the results being presented in Fig. 2 and Table 4. It should be noted that, for low [Hg^{2+}]$_{env}$ levels, a small increase in the [Hg^{2+}] concentration is quickly amplified by the *mer* GRC of the cell, leading to a quick increase in *mer* gene expression, which in turn will lead to a rapid increase in the mercury reduction rate (this process takes only a few minutes as revealed by the cell response to dynamic perturbations in Fig. 3). If one applies a step perturbation in [Hg^{2+}]$_{env}$ from 0.2 to 5 μM (i.e. a ratio of 25, Table 4), the step response in the *mer* enzyme synthesis displays an amplification ratio of 3908 for the control protein PmerR and of 523 for the other proteins (i.e. ET, PmerA, PmerD controlled by PmerR). The corresponding step increase in the Hg^{2+} reduction rate is in a ratio of 6425. However, this stimuli/response amplification effect exerted by the GmerR expression module diminishes quickly with the increase in the environmental [Hg^{2+}] level from 5 to 20 μM, and practically disappears being inhibited by a large amount of mercuric ion pollutant (the step increase in *mer* gene expression becoming half of the corresponding step increase in the external stimuli).

Conclusions

To model the mercuric ion reduction process in an *E. coli* cell, a satisfactory compromise between the detailing degree of process representation and the predictive capabilities has been realized using a mixture of Michaelis-Menten, Haldane, and Hill type kinetics completed with elementary reactions for regulatory steps of gene expression from the involved *mer*-operon. The derived structured dynamic model represents a progress vs. classical global rep-

T a b l e 4 – *Reaction rate increase and amplification of the mer operon expression by an increase in the mercuric ion environmental concentration.* [TF]$_s$ = 4 nM

Env. stimuli: [Hg^{2+}]$_{env}$ step increase (μM/μM)	Hg^{2+} reduction rate step increase (nM min^{-1}/nM min^{-1})	Cell response: Enzyme step increase (nM/nM)			
		PmerR	ET	PmerA	PmerD
5/0.2 = 25	25.7/0.004 = 6425	312.7/0.08 = 3908	3317/6.34 = 523	1868/3.57 = 523	52.4/0.1 = 524
20/5 = 4	71/25.7 = 2.76	887.8/312.7 = 2.84	6188/3317 = 1.86	3483/1868 = 1.86	94.5/52.4 = 1.80
40/20 = 2	82/71 = 1.15	1000/887.8 = 1.12	6572/6188 = 1.06	3700/3483 = 1.06	100/94.5 = 1.06
60/40 = 1.5	86/82 = 1.05	1036/1000 = 1.03	6689/6572 = 1.02	3766/3700 = 1.02	101.6/100 = 1.02
120/60 = 2	90/86 = 1.04	1071/1036 = 1.03	6800/6689 = 1.01	3828/3766 = 1.01	103.2/101.6 = 1.01

resentation of the mercuric ion reduction process. Besides, the used VVWC modelling framework appears to be a promising alternative to evaluate the GRC properties during simulation of system dynamic response. By placing seven regulatory modules (characterizing *mer* operon expression) in an *E. coli* growing cell, the bacterial mercury resistance via mercuric ion reduction can be studied by mimicking stationary or perturbed environmental conditions. By considering gene-expression modules together with the cell growth and its content replication, and by explicitly including lumped GRC interactions with the genome and proteome, other important effects can be modelled, such as the cell content 'inertial' effect in treating perturbations, and the effect of the indirect or secondary perturbations transmitted via the cell-volume under isotonic osmolarity conditions. The developed model is able to simulate some experimentally observed effects, such as: i) mercury transport and reduction rate inhibition with the substrate; ii) quick and efficient control exerted by the PmerR protein on individual *mer* gene expression; iii) cross- and self- control of the *mer* gene expression adjustable by means of dimeric TF levels; iv) gene expression amplification at low levels of inducer (mercuric ions); v) quantitative characterization of the GRC efficiency and simulation of cell response to external perturbations; vi) reproduce target GRC properties concerning the short rise-times of the activation/repressing proteins, key-species sensitivity to an external inducer, and synchronization in the target gene expression.

This paper suggests that, according to the available information and utilization scope, a suitable combination of lumped and elementary kinetic terms can be a promising modelling alternative to reproduce the GRC characteristics. Further developments of the whole-cell model are seeking supplementary details of the cellular process as soon as new experimental observations become available and cell component behaviour quantitatively pointed-out.

The modular modelling approach is proved appropriate to study the cell regulatory network, offering the advantage of an expandable simulation platform in accordance to the modelling purpose and available data. In such a manner, the individual but also holistic GRC properties can be studied, allowing a complete system characterisation in terms of stability, flexibility, multiplicity, efficiency, and robustness. Thus, the resulted GRC model can be useful in predicting the cell efficiency when coping with various loads of Hg(II)-ions, but also in assisting the *in-silico* design of a modified *E. coli* (cloned with plasmids), of higher efficiency, for improving the industrial bioprocess performance.

List of symbols

b – kinetic constant in (6)

c_j – species (individual, lump, or 'pool') concentration (nM, or cells L^{-1})

D – cell content dilution rate (i.e. cell-volume logarithmic growing rate)

$\mathbf{g}$ – kinetic model function vector

$\mathbf{J} = \mathrm{d}\mathbf{g}/\mathrm{d}\mathbf{c}$ – kinetic model Jacobian matrix

$\mathbf{k}$ – kinetic constant vector

K – equilibrium or kinetic constants

n – Hill-coefficient

n_j – species j number of moles

n_s – no. of species

N_A – Avogadro number, $6.022 \cdot 10^{23}$

r_j – species j reaction rate

R – universal gas constant

$s(y;x) = \partial y/\partial x$ – sensitivity of y vs. x

$S(y;x) = \partial \ln(y)/\partial \ln(x)$ – relative sensitivity of y vs. x

t – time

t_c – cell-cycle time

T – temperature

V – cell volume

Greeks

$\lambda(\mathbf{J})$ – eigenvalues of the dynamic model Jacobian

π – osmotic pressure

$\tau_{rec,j}$ – species j recovering time of the steady-state

τ_j – species j transition time from one steady-state to another

Index

cyt – cytoplasma

env – environment

max – maximum

0 – initial

ref – reference

s – steady-state

Superscript

T – transpose of a matrix

Abbreviations

$AVG(\tau_j)$ – average of τ_j

G• – gene

GRC – genetic regulatory circuit

In   – inducer

mer operon – mercury resistance operon

nM   – nmol L^{-1}, nano-mole (i.e. 10^{-9} mol L^{-1} concentration)

P• – protein

P.I. – performance index

Re() – real part

QSS – quasi-steady-state

$STD(\tau_j)$ – standard deviation of τ_j

TF   – transcription factor

tr() – trace of a matrix

VVWC – variable volume whole-cell

[.]   – concentration

References

1. *Barkay, T., Miller, S. M., Summers, A. O.,* FEMS Microbiology Reviews **27** (2003) 355.
2. *Brown, N. L., Stoyanov, J. V., Kidd, S. P., Hobman, J. L.,* FEMS Microbiology Reviews **27** (2003) 145.
3. *Hogan-Sheldon, J.,* Biological mercury reduction in the environment and its policy implications for metal regulations based on speciation, MSc Diss., Harvard College, Massachusetts Institute of Technology, 1995.
4. *Silver, S.,* FEMS Microbiology Reviews **27** (2003) 341.
5. *Cavet, J. S., Borrelly, G. P. M., Robinson, N. J.,* FEMS Microbiology Reviews **27** (2003) 165.
6. *Blencowe, D. K., Morby, A. P.,* FEMS Microbiology Reviews **27** (2003) 291.
7. *Solioz, M., Stoyanov, J. V.,* FEMS Microbiology Reviews **27** (2003) 183.
8. *Rensing, C., Grass, G.,* FEMS Microbiology Reviews **27** (2003) 197.
9. *Andrews, S. C., Robinson, A. K., Rodriguez-Quinones, F.,* FEMS Microbiology Reviews **27** (2003) 215.
10. *Schroder, I., Johnson, E., de Vries, S.,* FEMS Microbiology Reviews **27** (2003) 427.
11. *Mulrooney, S. B., Hausinger, R. P.,* FEMS Microbiology Reviews **27** (2003) 239.
12. *Kehres, D. G., Maguire, M. E.,* FEMS Microbiology Reviews **27** (2003) 263.
13. *Busenlehner, L. S., Pennella, M. A., Giedroc, D. P.,* FEMS Microbiology Reviews **27** (2003) 131.
14. *Nies, D. H.,* FEMS Microbiology Reviews **27** (2003) 313.
15. *Mergeay, M., Monchy, S., Vallaeys, T., Auquier, V., Benotmane, A., Bertin, P., Taghavi, S., Dunn, J., van der Lelie, D., Wattiez, R.,* FEMS Microbiology Reviews **27** (2003) 385.
16. *Lloyd, J. R.,* FEMS Microbiology Reviews **27** (2003) 411.
17. *Döbler, I. W., Canstein, H., Li, Y., Deckwer, W. D.,* Env. Sci. & Technol. **34** (2000) 4628.
18. *Deckwer, W. D., Becker, F. U., Ledakowicz, S., Wagner-Doebler, I.,* Environ. Sci. Technol. **38** (2004) 1858.
19. *Leonhäuser, J., Röhricht, M., Wagner-Döbler, I., Deckwer, W. D.,* Eng. Life Sci. **6** (2006) 139.
20. *Styczynski, M. P., Stephanopoulos, G.,* Comp. & Chem. Eng. **29** (2005) 519.
21. *Zak, D. E., Vadigepalli, R., Gonye, G. E., Doyle III, F. J., Schwaber, J. S., Ogunnaike, B. A.,* Comp. & Chem. Eng. **29** (2005) 547.
22. *Maria, G.,* Chemical and Biochemical Engineering Quarterly **21** (2007a) 417.
23. *Maria, G.,* Chemical and Biochemical Engineering Quarterly **19** (2005) 213.
24. *Maria, G.,* Chemical and Biochemical Engineering Quarterly **20** (2006) 353.
25. *Morgan, J. J., Surovtsev, I. V., Lindahl, P. A.,* Jl. theor. Biology **231** (2004) 581.
26. *Kinoshita, A., Nakayama, Y., Tomita, M.,* In silico analysis of human erythrocyte using E-Cell system, 2nd Int. Conf. on Systems Biology, California Institute of Technology (USA), Nov. 4, 2001.
27. *Kobayashi, H., Kaern, M., Araki, M., Chung, K., Gardner, T. S., Cantor, C. R., Collins, J. J.,* Proc. Natl. Acad. Sci. USA. **101** (2004**)** 8414.
28. *Philippidis, G. P., Malmberg, L. H., Hu, W. S., Schottel, J. L.,* Applied & Environmental Microbiology **57** (1991a) 3558.
29. *Philippidis, G. P., Schottel, J. L., Hu, W. S.,* Enzyme Microb. Technol. **12** (1990) 854.
30. *Philippidis, G. P., Schottel, J. L., Hu, W. S.,* Mathematical modelling and optimization of complex biocatalysis. A case study of mercuric reduction by *Escherichia coli,* Expression Systems & Processes for DNA Products, National Science Foundation Report ECE-8552670, University of Minnesota, 1991b.
31. *Philippidis, G. P., Schottel, J. L., Hu, W. S.,* Biotech. Bioeng. **37** (1991c) 47.
32. *Fehr, W.,* Biotransformation of thiomersal by naturally mercury resistant isolates and genetically engineered microorganisms, PhD Diss., TU Braunschweig (Germany), 2006.
33. *Sewell, C., Morgan, J., Lindahl, P.,* J. theor. Biol. **215** (2002) 151.
34. *Salis, H., Kaznessis, Y.,* Comp. & Chem. Eng. **29** (2005) 577.
35. *Maria, G.,* Quantitative risk evaluation of chemical processes and modelling of accident consequences, Printech Publ., Bucharest, 2007b (in Romanian).
36. *Yang, Q., Lindahl, P., Morgan, J.,* J. theor. Biol. **222** (2003) 407.
37. *EcoCyc,* Encyclopedia of Escherichia coli K-12 genes and metabolism, SRI Intl., The Institute for Genomic Research, Univ. of California at San Diego, 2005. http://ecocyc.org/
38. *Allen, G. C. Jr., Kornberg, A.,* Jl. Biological Chemistry **266** (1991) 11610.
39. *Rosenfeld, N., Elowitz, M. B., Alon, U.,* J. Mol. Biol. **323** (2002) 785.
40. *Voit, E. O.,* IEE Proc. Syst. Biol. **152** (2005) 207.
41. *Grainger, J. N. R., Bass, L.,* J. Theoret. Biol. **10** (1966) 387.
42. *Grainger, J. N. R., Gaffney, P. E., West, T. T.,* J. Theoret. Biol. **21** (1968) 123.
43. *Tomita, M., Hashimoto, K. Takahashi, K., Shimizu, T., Matsuzaki, Y., Miyoshi, F., Saito, K., Tanida, S., Yugi, K., Venter, J. C.,* Bioinformatics **15** (1999) 72.

44. *Tomita, M.,* Trends in Biotechnology **19** (2001) 205.

45. *Aris, R.,* Elementary chemical reactor analysis, Prentice-Hall, New Jersey, 1969.

46. *Wallwork, S. C., Grant, D. J. W.*, Physical Chemistry, Longman, London, 1977.

47. *Hlavacek, W. S., Savageau, M. A.,* J. Mol. Biol. **266** (1997) 538.

48. *Van Someren, E. P., Wessels, L. F. A., Backer, E., Reinders, M. J. T.,* Signal Processing **83** (2003) 763.

49. *Wall, M. E., Hlavacek, W. S., Savageau, M. A.,* J. Mol. Biol. **332** (2003) 861.

50. *Murray, J. D.,* Mathematical biology. An introduction, Springer Verlag, Berlin, 2001.

51. *Heinrich, R., Schuster, S.,* The regulation of cellular systems, Chapman & Hall, New York, 1996.

52. *Agrawal, P., Lee, C., Lim, H. C., Ramkrishna, D.,* Chemical Engineering Science **37** (1982) 453.

53. *Elowitz, M. B., Leibler, S.,* Nature **403** (2000) 335.

54. *Maria, G.,* Chemical and Biochemical Engineering Quarterly **18** (2004) 195.

55. *Buchholz, K., Hempel, D. C.,* Eng. Life Sci. **6** (2006) 437.

56. *Heinemann, M., Panke, S.,* Bioinformatics **22** (2006) 2790.